The toucan beak: Structure and mechanical response

Yasuaki Seki *, Bimal Kad, D. Benson, Marc A. Meyers

Department of Mechanical and Aerospace Engineering, University of California, San Diego, La Jolla, CA 92093-0411, USA

Available online 3 October 2005

Abstract

The structure and mechanical response of a Toco toucan (*Ramphastos toco*) beak were established. The beak was found to be a sandwich composite with an exterior of keratin scales (50 μm diameter and 1 μm thickness) and a core composed of fibrous network of closed-cells made of collagen. The tensile strength of the external shell is about 50 MPa. Micro- and nanoindentation hardness measurements corroborate these values. The keratin shell exhibits a strain-rate sensitive response with a transition from slippage of the scales due to release of the organic glue, at a low strain rate (5×10^{-5} s^{-1}) to fracture of the scales at a higher strain rate (1.5×10^{-3} s^{-1}). The closed-cell foam consists of fibers having a Young's modulus (measured by nanoindentation) of 12.7 GPa. This is twice as high as the keratin shells, which have $E = 6.7$ GPa. This is attributed to their higher calcium content. The compressive collapse of the foam was modeled by the Gibson–Ashby constitutive equations.

There is a synergistic effect between foam and shell evidenced by a finite-element analysis. The foam stabilizes the deformation of the keratin shell by providing an internal support which increases its buckling load under compressive loading.
© 2005 Elsevier B.V. All rights reserved.

Keywords: Toucan; Beak; Keratin; Foam; Viscoplastic; FEM

1. Introduction

The study of biological materials is inspiring new processing methods for materials. Examples such as silk, shell, spider web, and sea sponge spicule, abound. A fascinating class of biological materials is sandwich structures consisting of a solid shell and a cellular core; the cellular core increases the resistance of the shell to buckling, leading to a synergism between the two constituents. Plant stems and porcupine quills fall under this category.

Bird beaks are light-weight structures that need to possess significant specific strength and structure. The toucan has a long beak that is also thick, a necessity for food gathering in tall trees. This biological material can serve as a useful source for research and as an inspiration for structural design in engineering.

2. Experimental techniques

Toucan (*Ramphastos toco*) beaks (both the upper and lower parts), obtained after the natural death of animals from a local breeder, were used for mechanical tests and structural analysis. The black color region of the exterior beak was avoided because coloration has an effect on its hardness [1]. Humidity and temperature were measured because it is known that the mechanical properties are dependent on them.

Specimen preparation for nanoindentation and microindentation was the same. The toucan beak shell and foam were cut into small pieces by knife. Both samples were mounted in epoxy and glued on a glass plate. The experimental set up was the same as the one used earlier for hardness measurements of the starling beak [1]. A LECO M-400-H1 hardness testing machine with a load 100 gf was used. The indenter was applied for 15 s, and a subsequent 45 s was allowed to elapse before the diagonals of the indentation were measured. Since nanoindentation is highly sensitive to the roughness of the sample, specimens were polished to 0.05 μm. A Hysistron Triboindenter was used to determine the reduced Young's modulus and hardness of the exterior and interior. Loads of 500 and 1000 μN (Berkovich-type indenter) were applied to specimens.

The outer shell of the toucan beak was cut into rectangles with a knife to prepare tensile specimens. The rectangles were then inserted into a laser cutting machine and the dog bone shaped specimens were cut out (shape programmed into the

* Corresponding author. Tel.: +1 858 543 6091.
  E-mail address: yaseki@ucsd.edu (Y. Seki).

machine), with a length of 25.4 mm, width of 2.3 mm, gage length of 6.35 mm, and gage width of 0.5 mm. Longitudinal and transverse specimens were prepared. Since specimens had a preexisting curvature, a preload of 25 N was applied before initiating the test. A universal testing machine equipped with a 1000 N load cell was used. The displacement was measured with an extensometer attached to the grips. The tests were carried out at room temperature (23 °C) and humidity of approximately 50%. The specimens for compression testing of the foam were removed entirely (as one piece) from the beak by making cross sectional cuts with a high-speed diamond saw. Early attempts to cut parallelepipeds produced damage in the cellular material. The crosshead speed was 1.27 mm/min. For observation and characterization (Philips Scanning Electron Microscope), the keratin exterior of the beak and foam were coated with silver nitride.

In order to determine the main protein component of foam, amino acid analysis and hydrolysis were conducted with foam that was demineralized by 115 mM of HCl solution.

3. Results and discussion

3.1. Structure of the beak

Fig. 1(a) shows a photograph of the upper and lower parts of the beak. It has a density of approximately 0.1 g/cm^3, which enables the bird to fly while maintaining a center of mass at the line of the wings. The beak corresponds approximately to one third of the length of the bird, yet only makes up about 1/20 of its mass. The mesostructure and microstructure of the toucan beak reveal a material which is reminiscent of sandwich structures of functionally graded materials, with components made of foam covered by a hard surface layer. Fig. 1(b) shows the foam interior and three cross sections, at three positions along the beak length. Typical dimensions at a midway section along the beak are shown in Fig. 2.

Fig. 3(a) shows the exterior shell consisting of multiple layers of keratin scales. The thickness of each keratin scale is about 2~10 μm and the diameter is approximately 30~60 μm (Fig. 3(b)). The keratin scales are hexagonal and overlap each
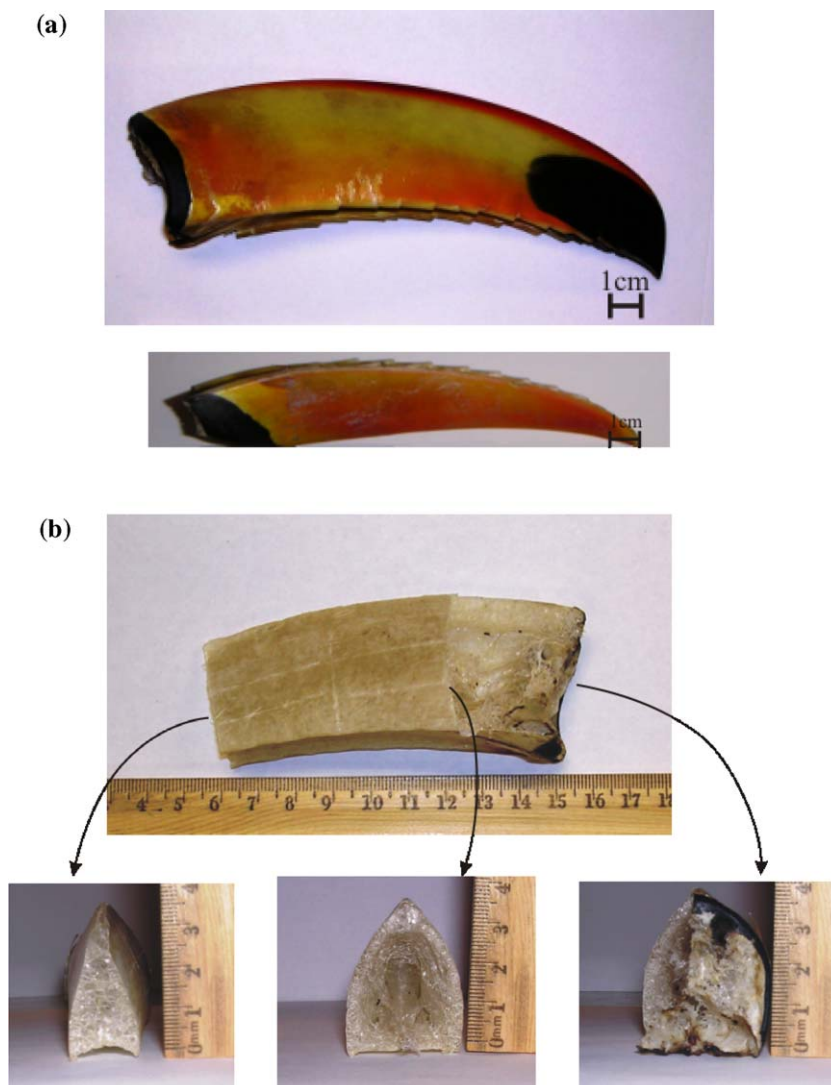

Fig. 1. Photographs of toucan beak; (a) toucan beak; (b) longitudinal view and cross sections of the foam.
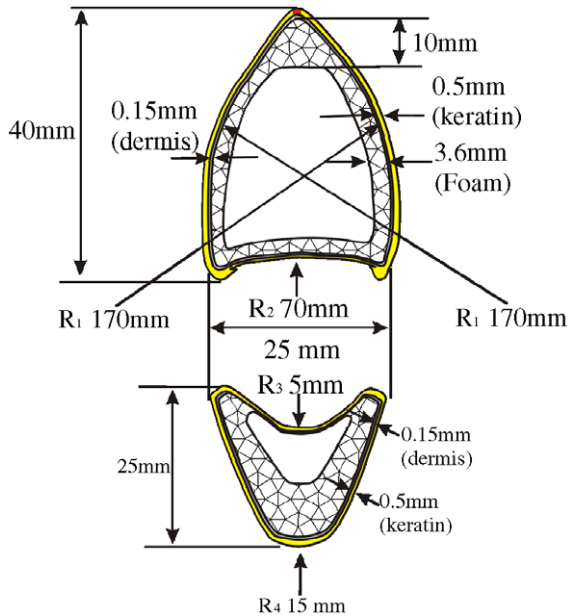
Fig. 2. Schematic cross section of toucan beak.

other. Although this was not investigated, they seem to be joined by a glue. The total shell thickness varies between approximately 0.5 and 0.75 mm. Beak keratin contains a relatively small amount of sulfur [2]. Fig. 3(c) shows the inside of the beak. It is clearly a foam structure. Most of the cells in

the toucan foam are sealed off by membranes with thickness of 2∼25 μm. Thus, it can be considered a closed-cell system. The cell sizes vary and the closed-cell network is comprised of struts with the thickness of 70∼200 μm with edge connectivity of three or four (Fig 3(d)).

Table 1 shows the amino acid analysis of the foam. One third of the components was glycine; it is typically found in bone structure. The results also suggested the toucan foam was made from a collagen. Thus, the foam seems to be made from bone and has the typical thin walled hollow tube structure of bone [3].

3.2. Mechanical properties of the beak

3.2.1. Micro- and nanoindentation

Table 2 shows a summary of mean hardness and reduced Young's moduli of the shell keratin and "bony" struts from foam. Although the same samples were tested, hardness from nanoindentation is twice as high as the one from microindentation. One of the possible reasons for the difference is the polishing of the surface, necessary for nanoindentation. However, the fibers in the foam were not polished and still exhibit higher values. There are reports of higher nanoindentation hardness than microindentation hardness for copper [4] and the same could hold true for keratin. They are explained by the pile-up effect and measuring method [4]. When it occurs, (as is the case with keratin and copper [4]) nanoindentation values are
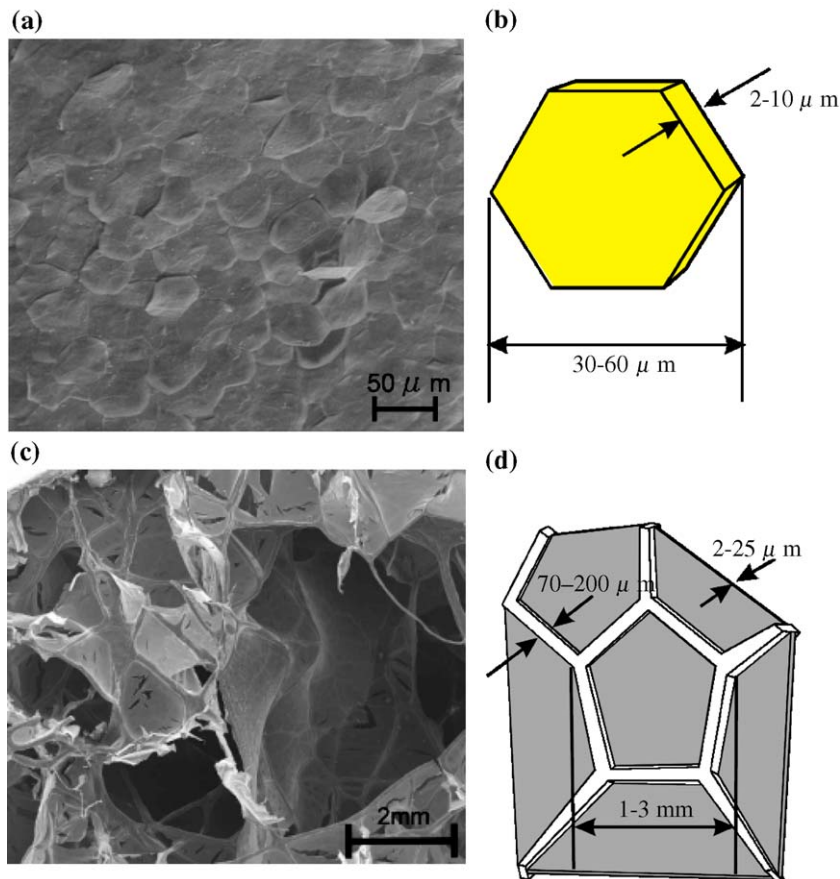

Fig. 3. Scanning electron micrographs and schematic drawings; (a) exterior of beak (keratin); (b) keratin scale; (c) interior of beak (foam); (d) closed cell of beak.

Table 1
Amino acid and acid hydrolysis results of the toucan foam

Amino acid	pmole analyzed	mol. %	Residue wt.	wt/wt. %
CYS02 (C)	0	0.00	151.2	0.00
HYP (Z)	1532	9.29	113.12	11.50
ASP (D)	817	4.95	115.09	6.24
THR (T)	349	2.12	101.11	2.34
SER (S)	560	3.39	87.08	3.23
GLU (E)	1282	7.77	129.12	10.99
PRO (P)	2072	12.56	97.12	13.36
GLY (G)	5321	32.26	57.05	20.15
ALA (A)	1892	11.47	71.08	8.92
VAL (V)	294	1.78	99.13	1.93
MET (M)	148	0.90	131.2	1.29
ILE (I)	209	1.27	113.16	1.57
LEU (L)	497	3.01	113.16	3.73
NLE	0	0.00	0.00	0.00
TYR (Y)	59	0.36	163.18	0.63
PHE (F)	204	1.24	147.18	2.00
HIS (H)	59	0.36	137.14	0.54
TRP	0	0.00	186.20	0.00
LYS (K)	460	2.79	128.18	3.91
ARG (R)	741	4.49	156.19	7.68
		100.00	Total ng	
Total pmole analyzed	16,495			

higher than microindentation. The pile-up effect occurred on the keratin surface and is described by Meyers and Chawla [5]. The higher nanoindentation values have also been discussed by Rho et al. [6,7] for bone and attributed to the scale of the collagen and mineral interactions.

3.2.2. Tensile and compressive response of beak

Typical tensile strain–stress curves of β-keratin from toucan beak, measured in longitudinal and transverse direction, are shown in Fig. 4(a). There was significant scatter in the results, which are shown in Table 3(a). There is no systematic difference between the Young's modulus and yield strength of keratin along the two directions. Mean values are 1.4 GPa (Young's modulus) and 30 MPa (yield strength). Thus, the keratin shell can be considered transversely isotropic.

Fig. 4(b) shows typical compressive stress–strain curves from toucan foam specimens. Young's modulus is determined by the initial slope of the curve. The plateau region is associated with the collapse of the cell walls. After the plateau, the densification of the cell wall starts. The crushing stress σ_{cr}* increased with the density of the foam. Mean value of crushing stress and Young's modulus are 0.17 MPa and 5.6×10^{-3} GPa, respectively. Densification starts at an approximate strain of 0.9. The spikes in the curve represent individual fracture events.

Table 2
Summary of mean micro and nano hardness and reduced Young' modulus

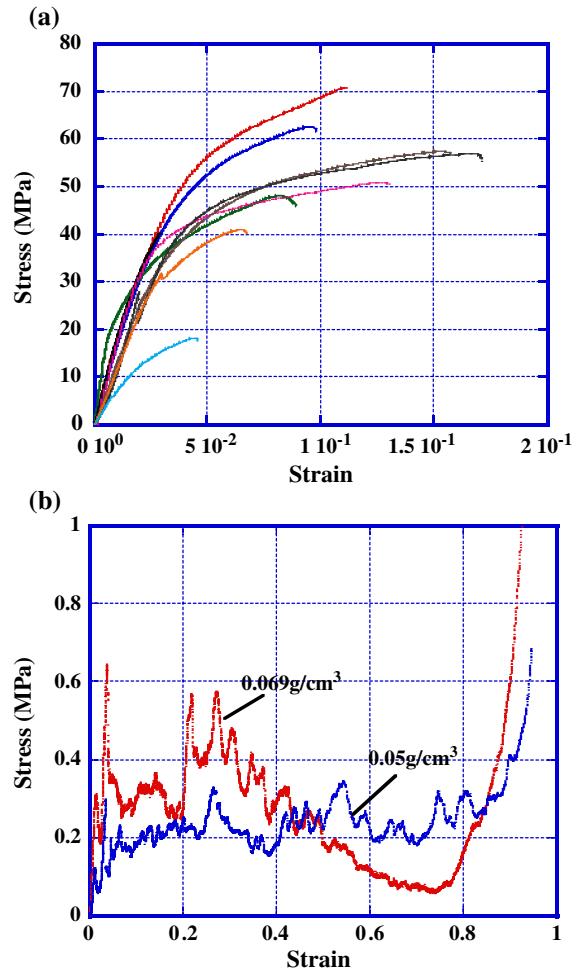|	Mean hardness (GPa) microindentation	Mean hardness (GPa) nanoindentation	Reduced Young's modulus (GPa)
Shell keratin	0.22	0.50	6.7
Fiber from foam	0.27	0.55	12.7

Fig. 4. (a) Tensile stress–strain curves for keratin shell; (b) compressive stress–strain curves for foam.

Keratin, a biological composite [8], shows two different fracture modes, dependent on the strain rate [9]. We observed that the keratin shell failure mode changes from scale pull-out to brittle fracture as the strain rate is increased. Fig. 5 presents the rationale for the failure mode change. The yield stress and UTS are plotted as a function of the strain rate. The yield stress is sensitive to the strain rate and associated with the viscoplasticity of the interscale glue. When the yield stress approaches (or exceeds) the UTS, fracture of the scales is preferred over viscoplastic deformation of the glue. The transition from pull out to scale fracture is governed by the criterion:

$$\sigma_t \leq \sigma_g \quad \text{or} \quad \sigma_t \geq g \tag{1}$$

where σ_t is the fracture stress and σ_g is the flow stress by interscale gliding. The strain rate dependence of σ_g can be expressed as:

$$\sigma_g = k\dot{\varepsilon}^m \tag{2}$$

where m is the strain rate sensitivity. This competition between viscoplastic shear of the interscale glue and tensile fracture of the scales is similar to the response exhibited by the abalone shell in tension [10]. In the case of abalone, the tiles are made of biomineralized aragonite.

Table 3
(a) Mechanical response (tension) of keratin shell, (b) crushing strength, density and plastic collapse strength of foam

(a) Mechanical response (tension) of keratin shell

	Strain rate (/s)	Young's modulus (GPa) (at strain 0.002)	Yield strength (MPa)	UTS (MPa)	Elongation (%)	Relative humidity %
1 Longitudinal	5×10^{-5}	1.1	24	45	11	47
2 Longitudinal	5×10^{-4}	1.0	31	41	7	55
3 Longitudinal	5×10^{-4}	1.2	28	57	16	55
4 Longitudinal	8×10^{-3}	1.8	35	51	14	48
5 Longitudinal	1.5×10^{-3}	1.9	43	59	8	47
6 Longitudinal	1.6×10^{-3}	0.85	17	32	17	48
Average	–	1.3±0.44	29.1±9.87	47.5±10.2	12.17±4.16	–
Transverse 1	5×10^{-4}	1.9	25	40	3	47
Transverse 2	5×10^{-4}	–	–	48	8	55
Transverse 3	5×10^{-4}	1.5	31	62	10	55
Transverse 4	8×10^{-4}	1.5	45	71	11	48
Average	–	1.633±0.23	33.6±10.26	55.25±14.25	8±3.5	–
Beak average	–	1.41±0.4	30.9±9.0	50.6±11.8	10.5±4.3	–

(b) Crushing strength, density and plastic collapse strength of foam

	Density (g/cm³)	Crushing Strength (MPa)	Young's modulus (GPa)	Relative density	Relative strength
Foam 1	0.031	0.065	4.6×10^{-4}	0.055	0.00071
Foam 2	0.039	0.08	2.1×10^{-3}	0.070	0.00087
Foam 3	0.05	0.225	7.0×10^{-3}	0.089	0.00247
Foam 4	0.069	0.325	1.3×10^{-2}	0.123	0.00357
Average	0.0473±0.016	0.174±0.124	5.6×10^{-3}±0.0056	0.095±0.029	0.00191±0.00137

The mechanical response of toucan beak keratin is similar to that of other bird keratins reported in the literature. The microhardness of the toucan beak is similar to that of the European starling [1]. The hardness of beak keratin is enhanced by mineralization [1,11]. The tensile response of the toucan beak keratin is analogous to the avian claw and it is not as stiff as feather keratin [12–14]. The structural organization of the beak keratin is also quite similar to the avian claw and distinct from feathers [15,16]. The tensile properties are isotropic along longitudinal and transverse directions (surface of beak). It is known that hydration significantly decreases stiffness and increases the ductility of keratin [17]. Our results are not sufficient to judge the effect of the humidity; this will be systematically investigated in the future.
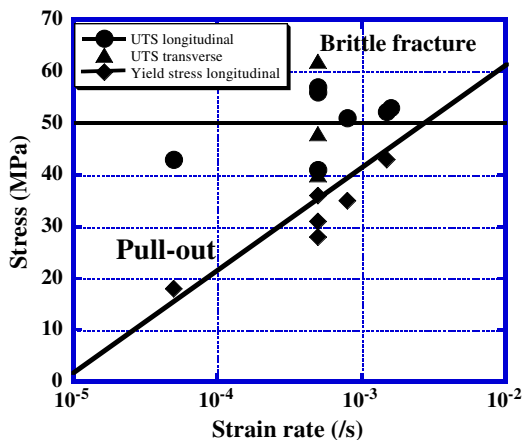

Fig. 5. Yield strength and UTS of shell keratin as a function of strain rate; notice two regimes of failure shown in figure.

3.3. Modeling of interior foam (Gibson–Ashby constitutive equations)

Gibson and Ashby [18] provide an analytical treatment for the mechanical behavior of a broad range of cellular materials. The most significant feature of the cellular solid is the relative density, ρ^*/ρ_s (density of the cellular material, ρ^*, divided by density of the solid material, ρ_s). The simplest closed-cell cubic model was introduced to describe the deformation of the foam. Fig. 6 shows (a) undeformed and (b) deformed cubic closed-cells envisaged by Gibson and Ashby [18]. The cubic array consists of the strut length l and thickness t_e. Each cell is sealed off by membrane thickness t_f. The closed-cell cubic is deformed by the compressive force F. The foams made from material possessing a plastic yield stress are subjected to plastic collapse when load beyond the linear elastic regime. When plastic collapse occurs, there is a long horizontal plateau in the stress-strain curve. Eq. (3) represents the response of a closed-cell foam schematically represented in Fig. 6:

$$\frac{\sigma^*_{pl}}{\sigma_{ys}} = C_5 \left(\phi \frac{\rho^*}{\rho_s} \right)^{3/2} + (1-\phi) \frac{\rho^*}{\rho_s} + \frac{p_0 - p_{at}}{\sigma_{ys}} \tag{3}$$

where σ^*_{pl} is the plastic collapse stress of foam, σ_{ys} is the yield stress of the solid portion, C_5 is a parameter, ϕ is the ratio of volume of face to volume of edge, p_0 is the initial fluid pressure, and p_{at} is the atmospheric pressure.

For the open-cell geometry, the parameter ϕ in Eq. (3) is equal to 1. Additionally, the pressure is unchanged, i.e.,
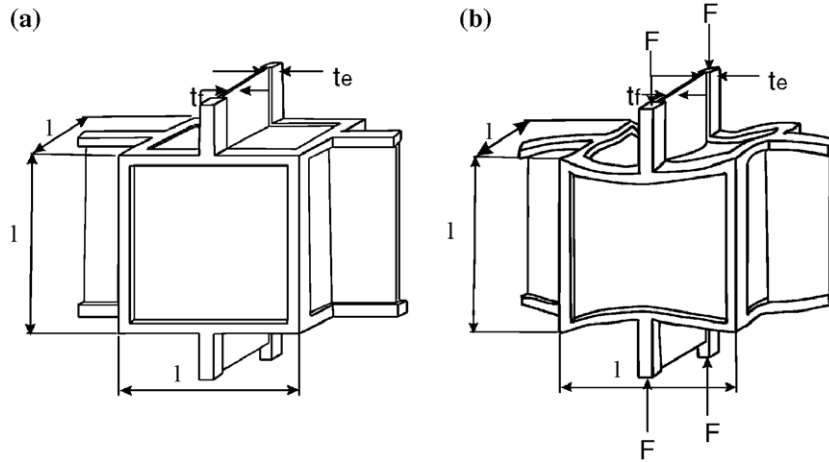
Fig. 6. (a) Gibson–Ashby model for closed-cell foam; (b) deformation of closed-cell foam.

$p_0 - p_{at} = 0$. Thus, Eq. (3) is reduced to the open-cell equation from Gibson and Ashby [18].

$$\frac{\sigma_{pl}^*}{\sigma_{ys}} = C_5 \left(\frac{\rho^*}{\rho_s} \right)^{3/2} \qquad (4)$$

The parameter C_5 has an experimentally obtained value [18] of 0.3 for plastic collapse and 0.2 for brittle crushing (where $\sigma_{pl}^* / \sigma_{ys}$ in Eqs. (3) and (4) is replaced by the normalized crushing stress $\sigma_{cr}^* / \sigma_{fs}$).

We carefully measured the density of the solid part of foam from six samples and found the density of solid was 0.56 g/cm^3. The density of the foam is 0.05 g/cm^3. Thus, the relative density of the toucan foam is approximately 0.1. The yield stress, σ_{ys}, is estimated from microindentation values ($H \approx 3\sigma_y$), which seem to be more accurate than the nanoindentation values due to the size effect. This gives a value of $\sigma_{ys} = 91$ MPa.

Fig. 7 shows the predictions from Eqs. (3) and (4) as well as experimental results for a number of materials [19–24]. These equations bracket the experimental results quite well. The relative yield stress for toucan foam is quite small because of

little contribution of the membranes. Most of the membranes contain defects and tears after the animal is dead. However, one would not expect this to be the case for the live animal. Gibson and Ashby [18] give values of $C_5 = 0.3$ and $C_5 = 0.2$ for plastic buckling and brittle crushing, respectively. The response of the toucan foam is intermediate between the two.
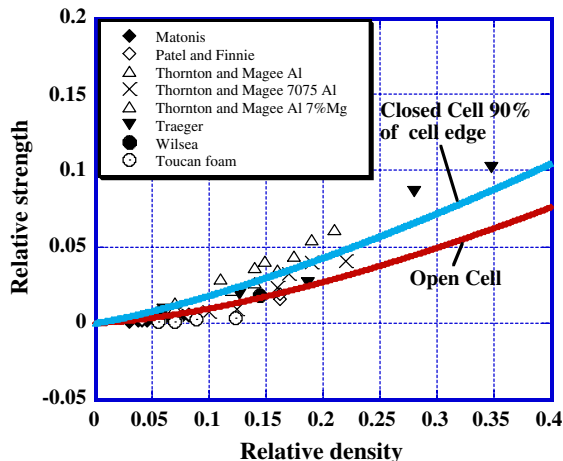

Fig. 8. Fracture morphology of closed-cell foam showing profuse foam strut bending; (a) overall view; (b) "green twig" fracture.

Fig. 7. Experimental results (hollow circles) and Gibson–Ashby prediction for open-cell and closed-cell foams (continuous lines).

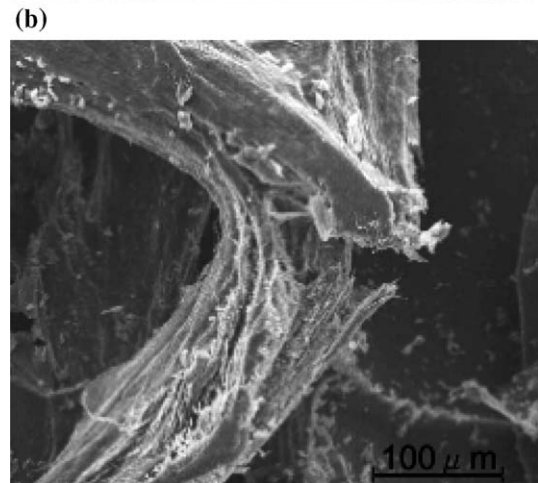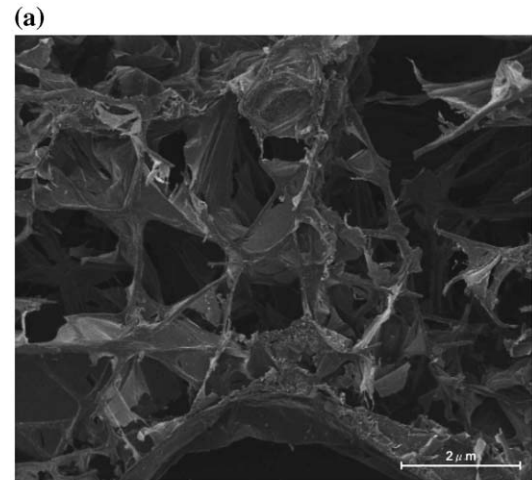Fig. 8(a) shows the fracture pattern of foam, consisting of a combination of partial and total fracture of foam ligaments. The foam ligaments have a fibrous structure similar to wood and can fracture partially when they are subjected to bending (Fig. 8(b)). The "green twig" appearance of the ligaments is evident in Fig. 8(b). Thus, the toucan foam does not crush completely and rather collapses in a semi-plastic manner.

3.4. FEM

Finite element analysis of the toucan beak using LS-DYNA [25] was performed to characterize the deformation pattern. Approximately 14,000 shell elements were used, and the stress–strain response was modeled with isotropic plasticity with linear hardening,

$$\sqrt{\frac{3}{2}\sigma' : \sigma'} = \sigma_y + h\varepsilon^p \tag{5}$$

where σ_y is the initial yield stress, h is the hardening exponent, and ε^p is the equivalent plastic strain. For the calculation shown here, E is 1.4 GPa, σ_y is 30 MPa, and h is 1 MPa. This corresponds to a good match with the experimental results.

The collapse of the shell, loaded in compression, is shown in Fig. 9. The shell (Fig. 9(a)) starts to deform and the applied stress folds it to the Fig. 9(b) condition. The shell is fully buckled in Fig. 9(c) and is completely crushed in Fig. 9(d). The mechanical response will be discussed later.

The foam was modeled with 8000 solid elements using a crushable foam model, material model 63 in LS-DYNA. Fig. 10(a) shows initial condition of the foam having a hollow region in the center. This shape reproduces the cross section of the beak, shown in Figs. 1 and 2. The deformed foam expands in the lateral direction, which produces shrinkage of hollow center, shown in Fig. 10(b). The crushable foam model used tabulated data from the actual compression tests to specify the nominal flow stress as a function of the volumetric strain in compression. The tabular data are also used in tension until the material reaches a tension cut-off, after which it is elastic-perfectly-plastic. Initially the stress is updated elastically each time step,

$$\sigma_{ij}^{Tr} = \sigma_{ij}^n + E\dot{\varepsilon}_{ij}\Delta t. \tag{6}$$

The three principal stresses, $\hat{\sigma}_i^{Tr}$, are obtained by an eigenvalue analysis, where $\hat{\ }$ indicates a principal value. If a
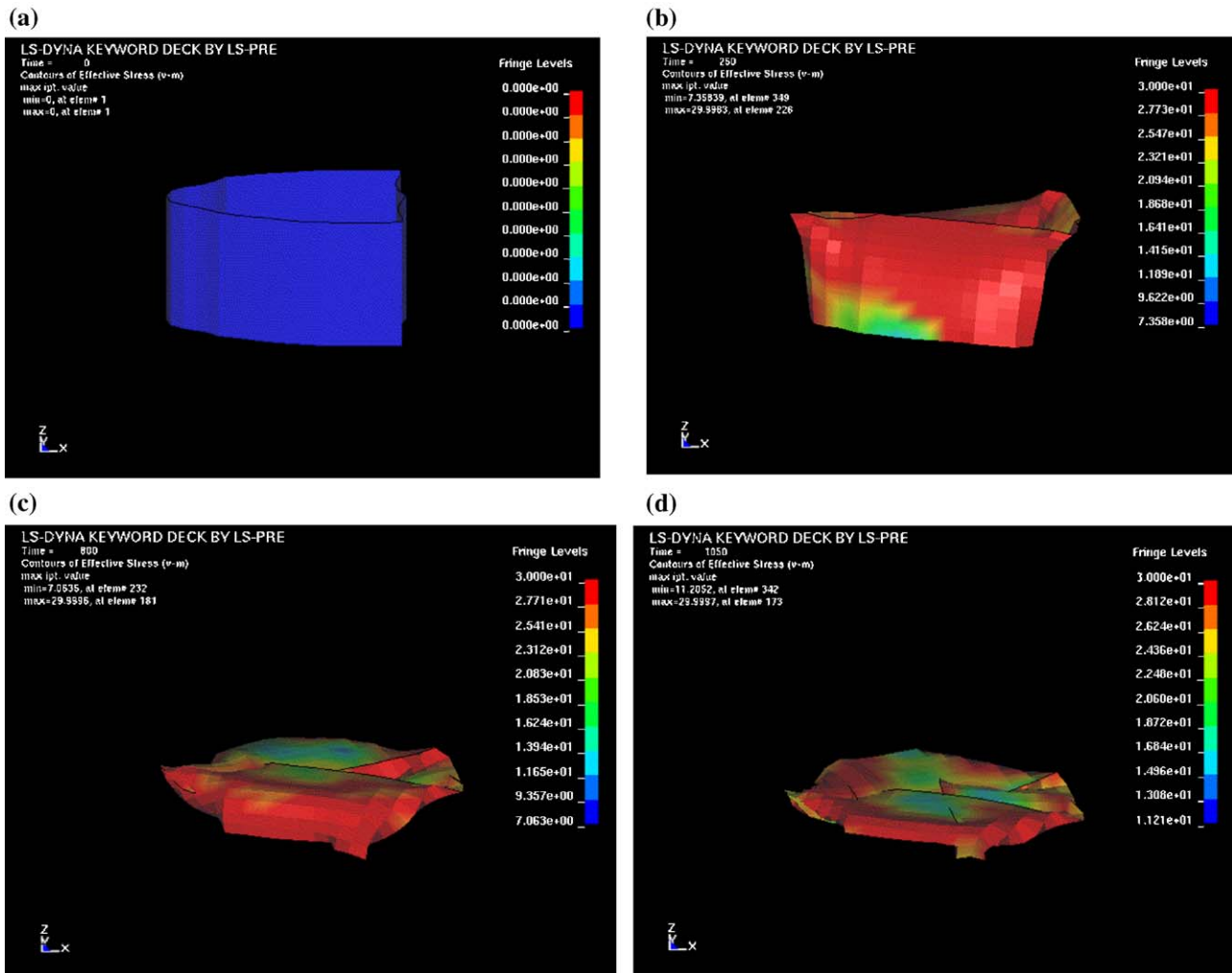

Fig. 9. FEM simulation of the beck shell under compression testing; (a) FEM model of shell; (b) onset od folding; (c) buckled shell; (d) completely collapsed shell.
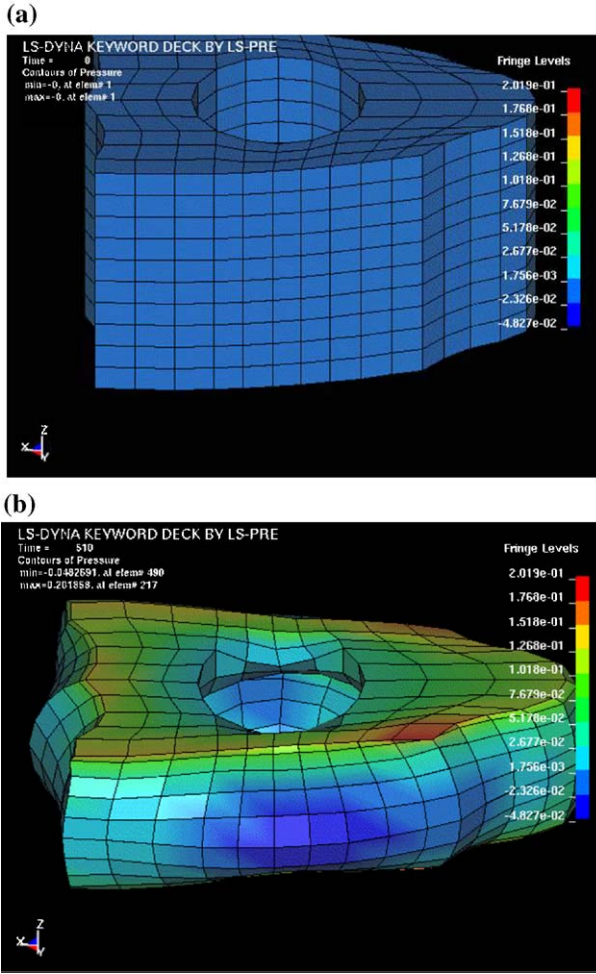
(a)

(b)

Fig. 10. FEM modelling of foam under uniaxial compression testing; (a) undeformed foam; (b) deformed foam.

principal value exceeds the yield stress, it is scaled back appropriately,

If $\sigma_y < |\hat{\sigma}_i^{\mathrm{Tr}}|$ then $\hat{\sigma}_i^{n+1} = \sigma_y \dfrac{\hat{\sigma}_i^{\mathrm{Tr}}}{|\hat{\sigma}_i^{\mathrm{Tr}}|}$, otherwise $\hat{\sigma}_i^{n+1}$

$$= \hat{\sigma}_i^{\mathrm{Tr}}. \qquad (7)$$

If plastic flow has occurred, the final stress tensor is

$$\sigma_{ij}^{n+1} = \sum_{i=1,3} \hat{\sigma}_i^{n+1} \Lambda_i \otimes \Lambda_i \qquad (8)$$

where Λ_i is the i-th eigenvector, otherwise the final stress is the stress updated elastically. For the current study, Young's modulus is 5.6×10^{-3} GPa, and the flow stress is 0.1 MPa.

Fig. 11(a) shows force-displacement curves of shells subjected to uniaxial compression testing. They were calculated by LS-DYNA; an experimental curve for a thickness of 0.6 mm is given for comparison. The compressive collapse of the shell was calculated for three thicknesses: 0.5, 1, and 2 mm. This is shown in Fig. 11(a) where the FEM and experimental results are compared. The maximum load is followed by a rapid decrease due to buckling. This computed response is analogous to the experimental result (shell thickness of 0.6 mm). The FEM

response shows a higher stiffness due to the lack of the imperfections and curvature. The experimentally determined and calculated responses of foam are shown in Fig. 11(b). The experimental results contain a larger number of spikes due to the individual fiber fracture events, while the FEM computation is smooth. The calculated and experimental results show a good match.

Fig. 11(c) shows the combined shell + foam response. The shell thickness is 0.4 mm for both, a value slightly lower than

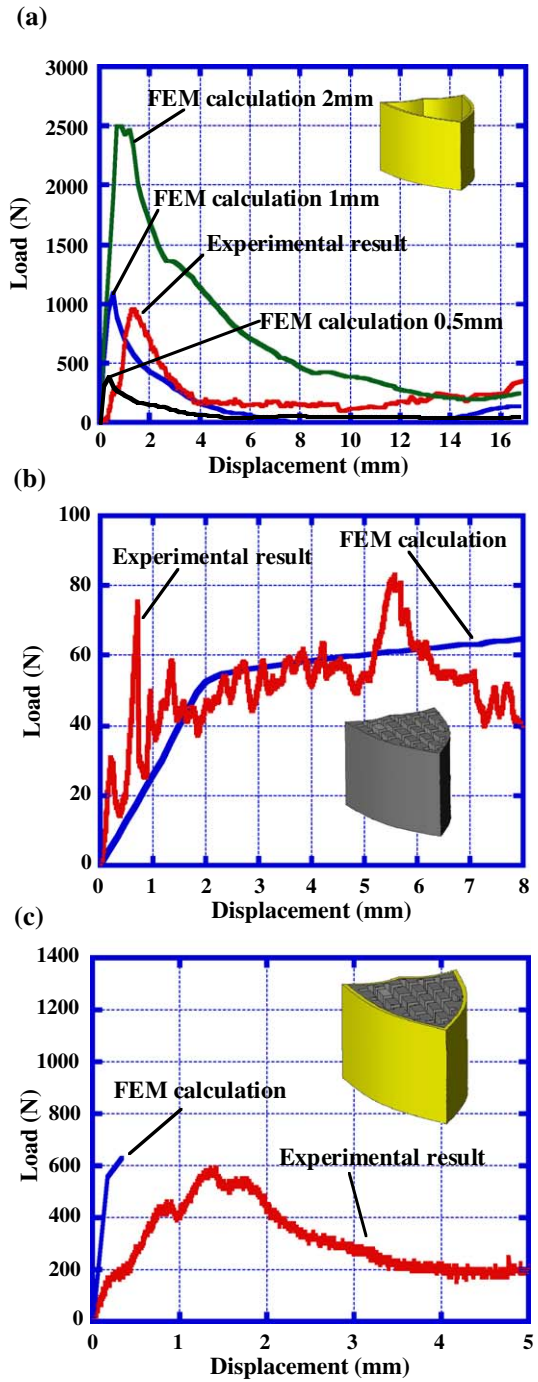**(a)**

(b)

(c)

Fig. 11. Comparison between Load vs. displacement curves from FEM calculation and experimental test results for thickness of 0.6 mm; (a) shell compression; (b) foam compression; (c) shell + foam compression (shell thickness: 0.4 mm).

the one in Fig. 11(a). The simulation shows that the presence of the foam prevents local buckling and therefore the load drop after the maximum is reduced. Thus, the stability of the structure is enhanced. This is a unique advantage of the sandwich structure. The foam corresponds to approximately 21% of the total weight. The calculations and experiments demonstrate that the deformation performance of the shell can be improved by using a foam core.

4. Conclusions

This study of the correlation between the mechanical properties and structure of the toucan beak reveals a synergism between the external keratin shell and the cellular interior with a hollow core which increases the stability of the structure. A detailed analysis of the synergism, based on the treatment by Karam and Gibson [26,27], is being published elsewhere [28]. The focus of the contribution whose results are presented herein is on the characterization and finite element modeling. The following are the principal conclusions:

- The beak microstructure was characterized and found to be composed of an external shell and an internal cellular core.
- The external shell consists of hexagonal keratin scales with a diameter of approximately $30–60$ μm and thickness of $2–10$ μm. These keratin scales are arranged in a staggered pattern; the total thickness of the shell is $0.5–0.75$ mm.
- The inside of the beak consists of a closed-cell foam with density of 0.05 g/cm^3. The ligaments of the closed-cell foam have a density of 0.56 g/cm^3 and are made of collagen. Thus, the relative density of toucan foam is 0.1.
- The keratin shell exhibited a strain-rate dependent failure: at 5×10^{-5} s^{-1}, failure occurs by pullout of the scales; at 1.5×10^{-3} s^{-1}, failure takes place by fracture of the scales. This strain rate dependence of the failure mode could be due to the viscoplastic nature of the glue.
- The toucan foam collapses by a mixture of brittle crushing and ductile bending of ligaments. The Gibson–Ashby constitutive equation for a closed-cell configuration describes this response well.
- The finite element method demonstrates that the compressive buckling loads for the sandwich structure of the beak is higher than shell alone. This is due to the stabilizing effect exerted by the foam on the thin shell, retarding its collapse.

Acknowledgements

References

[1] R.H.C. Bonser, M.S. Witter, Condor 95 (1993) 736.
[2] M.J. Frenkel, J.M. Gillespies, Aust. J. Biol. Sci. 29 (1976) 467.
[3] J. Curry, The Mechanical Applications of Bones, Princeton University Press, 1984.
[4] L. Qian, M. Li, Z. Zhou, H. Yang, X. Shi, Surf. Coat. Technol. 195 (2005) 264.
[5] M.A. Meyers, K.K. Chawla, Mechanical Metallurgy, Prentice Hall, New Jersey, 1984, p. 619.
[6] J.Y. Rho, M.E. Roy, T.Y. Tsui, G.M. Pharr, Transactions of the 43th Annual Meeting of the Orthopaedic Research Society, San Francisco, CA, 1997, p. 811.
[7] J.Y. Rho, K.S. Liisa, P. Zioupos, Med. Eng. Phys. 20 (1998) 92.
[8] R.D. Fraser, T.P. Macrae, The Mechanical Properties of Biological Materials: Symp Soc Exp Biol, vol. 34, Cambridge Press, Cambridge, 1980, p. 211.
[9] M.A. Kasapi, J.M. Gosline, J. Exp. Biol. 199 (1996) 1133.
[10] A. Lin, M.A. Meyers, Mater. Sci. Eng. 390 (2005) 27.
[11] F.G.E. Pautard, Nature 199 (1963) 531.
[12] R.H.C. Bonser, P.P. Purslow, J. Exp. Biol. 198 (1995) 1029.
[13] R.H.C. Bonser, J. Mater. Sci. Lett. 19 (2000) 1039.
[14] C.J. Cameron, T.J. Wess, R.H.C. Bonser, J. Struct. Biol. 143 (2003) 118.
[15] A.H. Brush, Biochem. Syst. Ecol. 14 (1986) 547.
[16] A.H. Brush, J.A. Wyld, Comp. Biochem. Physiol. 73B (1982) 313.
[17] R.H.C. Bonser, J. Mater. Sci. Lett. 21 (2002) 1563.
[18] L. Gibson, M.F. Ashby, Cellular Solids: Structure and Properties, 2nd ed., Cambridge University Press, 1997.
[19] R.K. Traeger, J. Cell. Plast. 3 (1967) 405.
[20] V.A. Matonis, Soc. Plast. Eng., J. (1964 (September)) 1024.
[21] P.H. Thornton, C.L. Magee, Met. Trans. 6A (1975) 1253.
[22] P.H. Thornton, C.L. Magee, Met. Trans. 6A (1975) 1801.
[23] M. Wilsea, K.L. Johnson, M.F. Ashby, Int. J. Mech. Sci. 17 (1975) 457.
[24] M.R. Patel, I. Finnie, J. Mat. 5 (1970) 909.
[25] Livermore Software Technology Corporation, LS-DYNA Keyword User's Manual, 2003.
[26] G.N. Karam, L.J. Gibson, Int. J. Solids Struct. 32 (1995) 1259.
[27] G.N. Karam, L.J. Gibson, Int. J. Solids Struct. 32 (1995) 1285.
[28] Y. Seki, M.S. Schneider, M.A. Meyers, Acta Mat. (in press).